

Variation of whitecap coverage with wave-field conditions

Y. Sugihara ^{a,*}, H. Tsumori ^a, T. Ohga ^a, H. Yoshioka ^b, S. Serizawa ^c

^a Department of Earth System Science and Technology, Kyushu University, Kasuga 816-8580, Japan

^b Department of Applied Information Science and Technology, Aichi Prefectural University, Aichi 480-1198, Japan

^c Disaster Prevention Research Institute, Kyoto University, Wakayama 649-3502, Japan

Received 8 October 2005; accepted 8 January 2006

Available online 27 September 2006

Abstract

Field observations were carried out at a sea observation tower to investigate how whitecap coverage on the ocean surface responds to wave-field conditions. Images of whitecaps were taken for every 4 h or 7 h in the daytime using a 3CCD digital video camera fixed at 14 m elevation, and they were stored automatically in a hard disk video recorder at a time interval of 1 s. The determination of whitecap coverage was made by means of a digital image processing. The 1/3 power of whitecap coverage increases linearly with increasing the 10-m neutral wind speed. On the basis of the deflection angle between the propagating directions of wind waves and swell, wave-field conditions are classified into four cases. The present results show that whitecaps are produced most actively under the condition of the pure windsea and they tend to be suppressed by the presence of swell. It is difficult to find a certain relation between the deflection angle and whitecap coverage. Whitecap coverage also increases with the wave age in the same wind-speed conditions.

© 2006 Elsevier B.V. All rights reserved.

Keywords: Whitecap coverage; Wave breaking; Wind waves; Swell; Wave age; Image processing

1. Introduction

Wave breaking plays an important role for the exchanges of momentum, heat and gas across the air–sea interface because it enhances turbulence at the interface and the entrainment of bubbles. Whitecap coverage, which is defined as the area of whitecaps per unit sea surface, has become of interest as one of the indexes to quantify wave breaking at the ocean surface. Monahan (1993) proposed the idea which is to distinguish the area of whitecaps according to 256 different levels of the surface brightness in grayscale images of the sea surface.

After his study, a digital image processing has frequently been used for the estimation of whitecap coverage. He found a cube law between whitecap coverage and wind speed as follows:

$$W_C = c_1(U_{10} - c_0)^3, \quad (1)$$

where W_C (%) indicates whitecap coverage, U_{10} the 10-m wind speed, and c_0 and c_1 denote empirical constants. This expression has been supported widely by many other researchers.

Zhao and Toba (2001) reanalyzed previous observational data of whitecap coverage by using various wind–wave parameters such as the wave age $g/\omega_p u_*$ and a breaking-wave parameter R_B ($\equiv u_*^2/v_a \omega_p$) proposed by Toba and Koga (1986), where u_* is the air friction

* Corresponding author.

E-mail address: sugihara@esst.kyushu-u.ac.jp (Y. Sugihara).

velocity, g the acceleration of gravity, ν_a the kinematic viscosity of air and ω_p the spectral peak angular frequency of wind waves. They showed a good correlation between W_C and R_B to be established and gave the following relation:

$$W_C = 3.88 \times 10^{-5} R_B^{1.09}. \quad (2)$$

They also examined the relation between W_C and a Reynolds number R_H given by $u_* H_s / \nu_a$ with H_s being the significant wave height, which was used as a characteristic lengthscale of turbulent boundary layer beneath the windsea. Based on observational data, an empirical relation

$$W_C = 4.02 \times 10^{-5} R_H^{0.96} \quad (3)$$

was obtained. These relations seem to be noticeable from the viewpoint of use of dimensionless parameter connected with wave breaking. The validity of the relations should be confirmed in detail through the comparison with observational data taken more accurately. In order to predict accurately whitecap coverage, [Stramska and Petelski \(2003\)](#) investigated the variation of the coverage with information on surface waves by analyzing digital camera images taken from a vessel in Arctic Ocean, North Atlantic. They pointed out that the correlation between whitecap coverage and wind speed is significantly affected by the development of surface waves, whereas it is seldom affected by the air stability and the water temperature. [Lafon et al. \(2004\)](#) measured whitecaps in a coastal zone and investigated characteristics of whitecap coverage in terms of the wind and wind–wave parameters. They showed that there exist two distinct portions in the behavior of whitecap coverage against the wave age, and that the behavior is similar to those of the drag coefficient and the wave growth rate. They also mentioned the possibility that the friction velocity can express the effects of the steady and unsteady wave conditions on whitecap coverage. Thus, the previous studies suggest that whitecap coverage depends strongly on characteristic quantities of the state of surface waves. However, how whitecap coverage depends on the wave age and the presence of swell has not been clarified sufficiently because of the lack of whitecap data with information on wave-field conditions.

Parameterizations of air–sea fluxes have often been attempted on the basis of whitecap coverage. [Monahan \(1993\)](#) distinguished the whitecapping area appearing in wave crests, where waves break actively, from the region of suspended bubbles in the rear of breaking waves. He stated that the transfers of energy and momentum are dominated mainly in the region of wave crests. Taking

account of the difference between the gas transfer velocities at the non-breaking surface and the breaking one, [Monahan and Spillane \(1984\)](#) proposed an empirical relation of the gas transfer velocity k_L as follows:

$$k_L = k_M(1-W) + k_W W, \quad (4)$$

where W is the fractional whitecap coverage, and k_M and k_W are the gas transfer velocities at the non-breaking surface and the breaking one, respectively. [Asher et al. \(1995\)](#) also derived the following relation, in which the transfer velocity k_W of Eq. (4) is separated into the contributions due to turbulence k_T and due to bubbles k_B :

$$k_L = \{k_M + W(k_T - k_M)\} + Wk_B. \quad (5)$$

[Asher and Wanninkhof \(1998\)](#) examined carefully the dependence of k_M , k_T and k_B on the 10-m wind speed, and proposed an empirical expression of the gas transfer velocity such as

$$k_L = \{47U_{10} + W(115, 200 - 47U_{10})\} Sc^{-\frac{1}{2}} + W(-37/\alpha + 6120\alpha^{-0.37} Sc^{-0.18}) \quad (6)$$

for k_L in units of centimeters per hour and U_{10} in meters per second, where Sc and α are the Schmidt number and the Ostwald solubility of the gas, respectively. The first term on the right-hand side indicates a turbulent effect associated with the wind and wave breaking, and the second term is a soluble effect from the inside of bubbles into the seawater. The following relation was determined from observational data obtained in GasEx-98 (see [Asher et al., 2002](#)):

$$W = 3.7 \times 10^{-6} (U_{10} - 1.2)^3. \quad (7)$$

Substitution of Eqs. (7) to (6) gives the relation between the gas transfer velocity and whitecap coverage. [Asher et al. \(2002\)](#) pointed out that the behavior of such a relation was similar to that of observational data in an open sea obtained by [McGillis et al. \(2001\)](#). [Woolf \(2005\)](#) estimated the gas transfer velocity on the basis of the separation of “breaking” and “non-breaking” contributions. The transfer velocity due to “breaking” contribution was parameterized by using whitecap coverage. For the parameterization, he considered that whitecap coverage should be affected by not only the wind speed but also wave-field conditions. In addition, he pointed out the importance of swell for the whitecapping, and made the parameterization of whitecap coverage in terms of a Reynolds number including the contribution of swell defined as $u_* H_s / \nu_w$ with ν_w being the kinematic viscosity of water. These results show whitecap coverage to be a useful parameter to quantify the gas transfer velocity.

Many sea surface images obtained in previous studies have been taken from vessels, so that their declinations have been inevitably small. In such cases, there exists much difference between whitecap coverage for the photograph taken from the front of waves and that for the photograph taken from the back. Therefore, in order to establish the quantification method for whitecap coverage, it is important to obtain sea surface images taken from the position just above the surface and to collect the data concerning wave-field conditions.

The purpose of this study is to make clear how whitecap coverage responds to wave-field conditions. Digital images of the sea surface were taken at a sea observation tower, and whitecap coverage was estimated accurately as the mean value over 600 images. The influence of swell on whitecap coverage is investigated on the basis of the deflection angle between the propagating directions of wind waves and swell, which were obtained from directional frequency wave spectra. In addition, the dependence of whitecap coverage on the wave age is examined.

2. Field site and observations

Field observations were carried out from November 5 to December 9, 2003 (observation A) and February 13 to March 5, 2004 (observation B), at a storm surge observation tower of the Shirahama Oceanographic Observatory of Kyoto University. It is located in the west region of Tanabe Bay, Wakayama, Japan and 2 km off the nearest coast. Fig. 1 shows a map around the observation tower. The mean water depth is about 30 m deep; however the tower is mounted on a hump at about 10 m deep. Since the hump is relatively small, swells come to the tower almost without being influenced by the hump. There is an open sea in the direction of the southwest, so that a relatively large swell propagates mainly from the southwest.

Fig. 2 shows a schematic diagram of observation system attached to the tower. Wind speeds were measured at a sampling rate of 10 Hz by using a three-component ultrasonic anemometer, which was mounted 23 m above the mean sea level. They were averaged over 10 min to obtain the mean wind speeds and wind directions. The friction velocities u_* were calculated on the basis of the inertial dissipation method. According to the profile method, wind speeds at an elevation of 10 m U_{10} were estimated from the mean wind speeds and the friction velocities at 23 m. The air temperature at 16 m height from the sea level T_a and the sea surface temperature T_s were measured in steps of 30 s to provide the near-water air stability $\Delta T (= T_a - T_s)$. The air pressure,

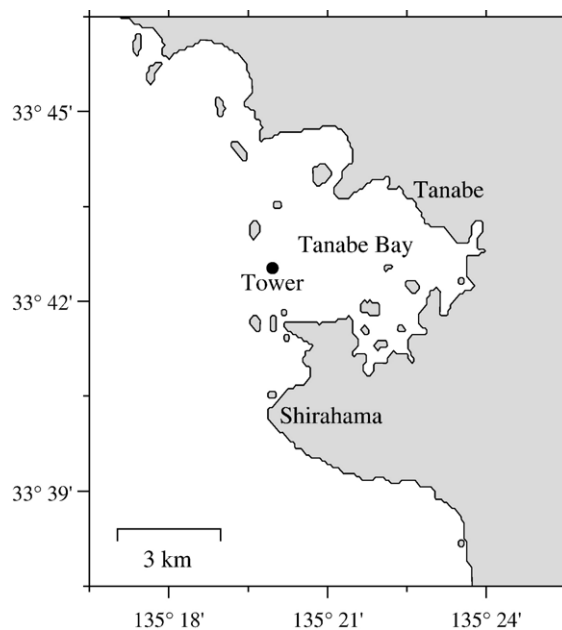


Fig. 1. Location of storm surge observation tower of the Shirahama Oceanographic Observatory.

water level and water temperature were also measured continuously at a time interval of 30 s. An acoustic Doppler current profiler (WAVEADCP) was located on the sea bed at a distance 20 m apart from the tower. Statistical wave characteristics such as the significant wave height H_s , the spectral peak period of waves T_p and the directional frequency wave spectra were estimated from the WAVEADCP data.

Digital images of whitecaps were taken in the daytime for every 7 h (8:30–15:30) during the observation A or 4 h (7:30–11:30) during the observation B, by using a 380,000 pixels 3CCD digital video camera (SONY DXC-390) located at 14 m height from the sea level. They were stored automatically in a hard disk video recorder (SONY HSR-X200) in steps of 1 s. The camera was put in a camera housing to protect it from the rain and seawater spray. In order to take pictures of the sea surface above the WAVEADCP, the azimuth and the declination angle of the camera were set to 215° and 33°, respectively. The photographic region calculated from the focal length of the camera was about 24 m long \times 15 m wide.

3. Digital image processing

Whitecap coverage is defined as the area of whitecaps per unit sea surface. A digital image processing carried out in this study is as follows. First, digital images of the sea surface obtained from the observations were taken into a computer, and the color original

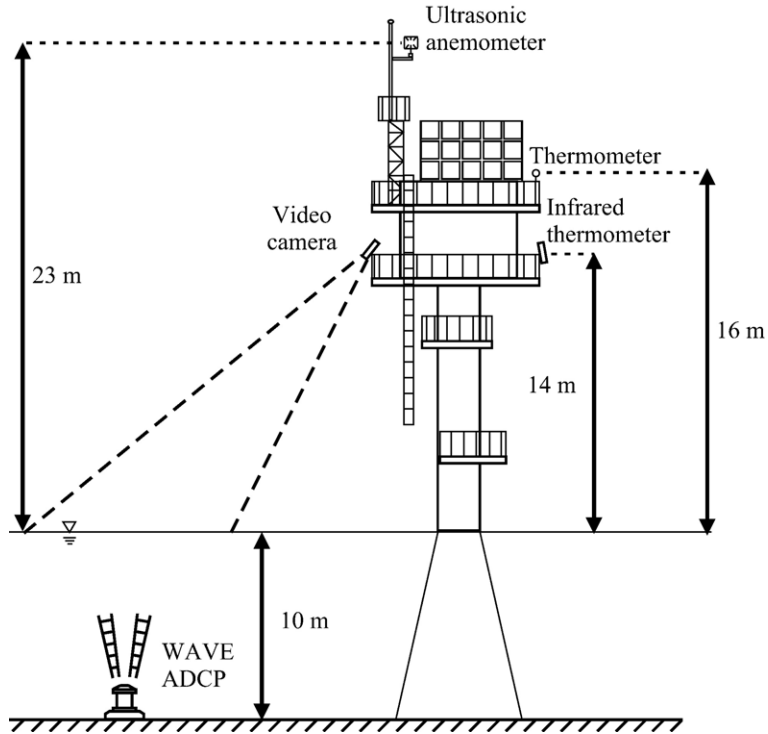


Fig. 2. Schematic diagram of observation system.

images were changed into grayscale ones of 256 gradation sequences. Next, a threshold level of the sea surface brightness was determined so as to identify the whitecapping area. The number of pixels in the whitecapping area divided by that in the whole analytical area were computed in steps of 1 s as an

instantaneous value of whitecap coverage. Since the brightness of the sea surface varied through the observations, the threshold level and the analytical area were changed every 10 min. In this study, the analysis was conducted mainly for the images in cloudy weather conditions of the little reflection of the sunlight.

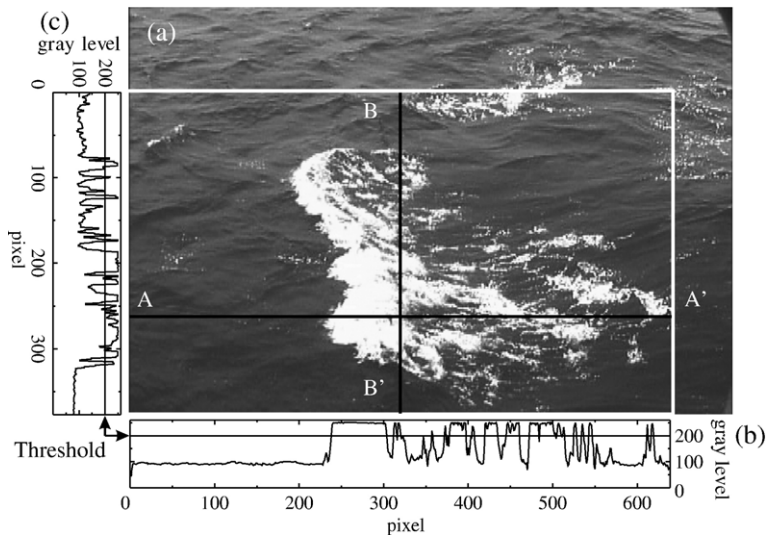


Fig. 3. Picture of whitecaps. (a) Grayscale image. (b) Distribution of brightness on A–A' line. (c) Distribution of brightness on B–B' line.

Finally, whitecap coverage was averaged over 600 images, which means the averaging was over 10 min.

Fig. 3 (a) shows an example of the grayscale image of whitecaps on the sea surface. Within the frame of white lines has been made the image processing. The resolution of the whole image area is 710×478 pixels, while that of the analytical area is 639×377 pixels. Fig. 3 (b) and (c) denote the brightness distributions along the A–A' and the B–B' lines shown in Fig. 3 (a), respec-

tively. The value of the threshold for this image takes 200. The brightness increases dramatically in the white-capping area compared with the background.

In order to examine the change in whitecap coverage by the threshold level, the binary images and the values of whitecap coverage W_C are shown in Fig. 4, where the threshold has been changed to five cases (140, 165, 175, 185, 240) and whitecap coverage has been computed within the frame of white lines. From this figure, the

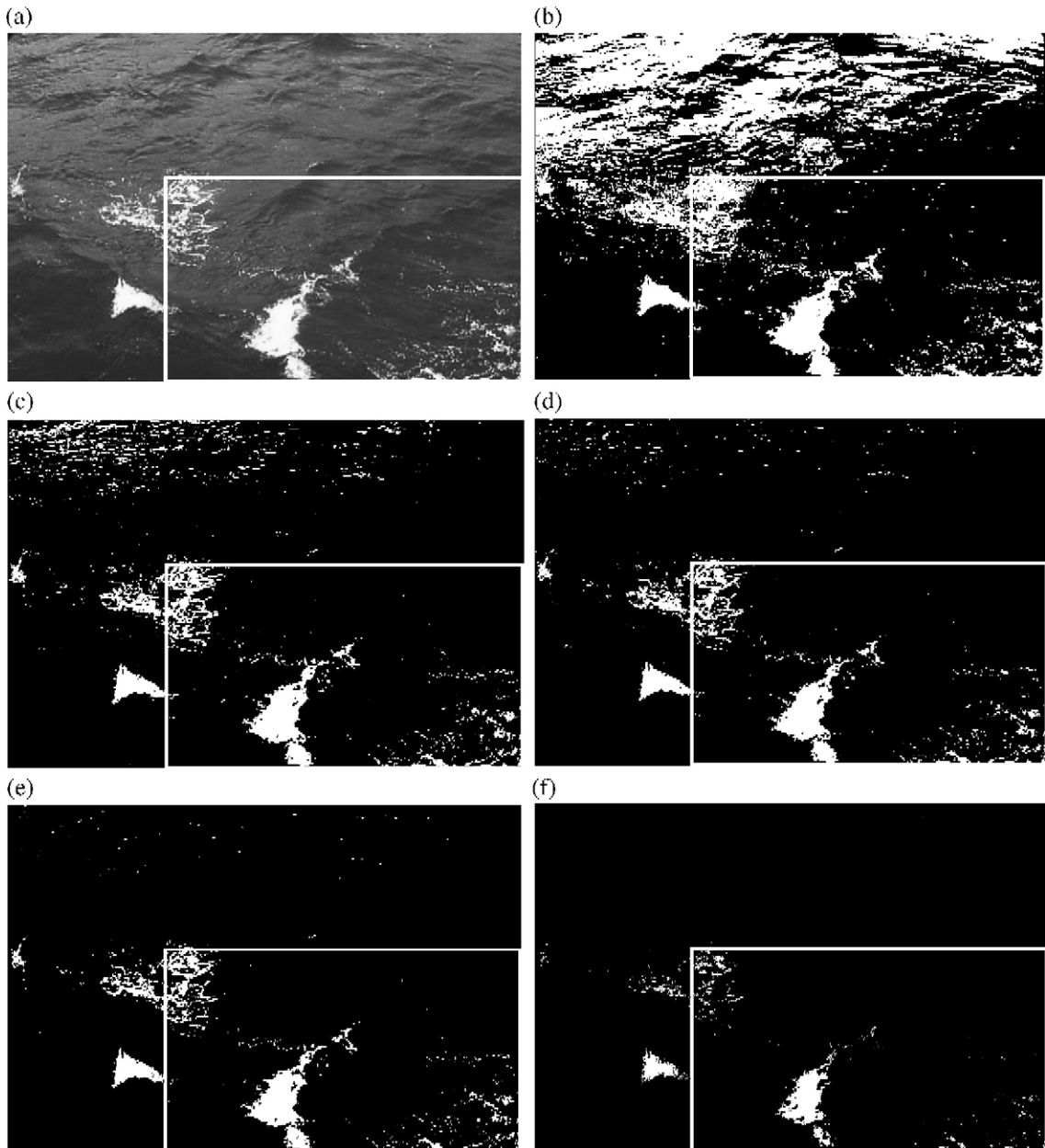


Fig. 4. Variations of binary images with the threshold level. (a)Original image, (b)Threshold=140, $W_C = 12.8\%$, (c)Threshold=165, $W_C = 8.83\%$, (d)Threshold=175, $W_C = 7.93\%$, (e)Threshold=185, $W_C = 7.23\%$, (f)Threshold=240, $W_C = 3.21\%$.

brightness of the sea surface is found to be relatively high in the upper part of the picture because of the influence of the sunlight. Under the condition of the threshold of 140, the non-whitecapping area is recognized as the whitecapping one, whereas for the threshold of 240, the area thought to be whitecaps cannot be identified suitably. In practice, the threshold for this time zone was set to 175. Since whitecap coverage at the threshold of 175 becomes 7.93%, and the relative error against the change of ± 10 thus is found to be about 10%. Whitecap coverage may increase extremely when the sunlight affects the images. In this study, so as to remove the influence of the sunlight through 600 images, the analytical area was set up more smallish and the threshold level was set up more largish.

Fig. 5 (a) indicates how whitecap coverage varies with the threshold for the image shown in Fig. 4, where the threshold has been changed in steps of 5. This figure shows that whitecap coverage almost remains about 100% until the threshold of 100 and it decreases rapidly in a range where the threshold exceeds 100. When the

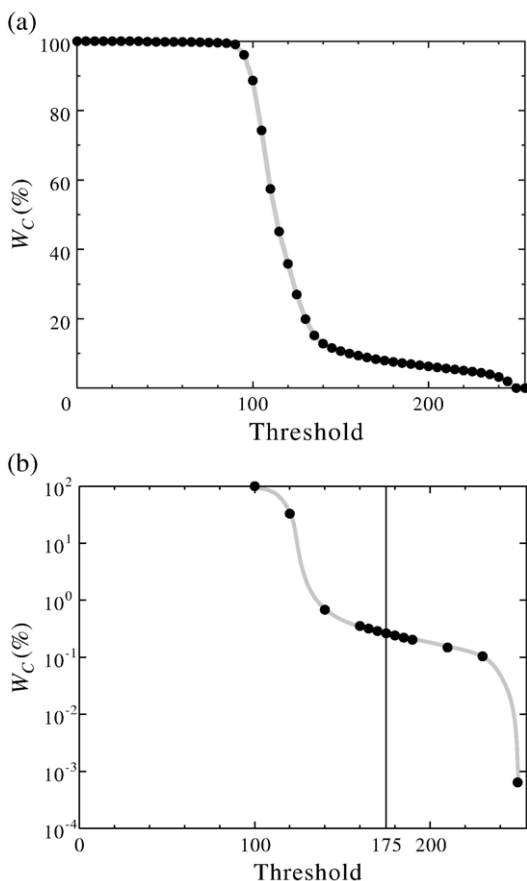


Fig. 5. Change in whitecap coverage by the threshold. (a) Instantaneous whitecap coverage. (b) Whitecap coverage averaged over 10 min.

threshold exceeds 140, whitecap coverage begins again to decrease much gradually and it becomes almost 0% at the threshold of 250. The former corresponds to the brightness range of the non-whitecapping area, where the reflection of the sunlight is dominant, while the latter is attributable to the brightness difference between the whitecapping and non-whitecapping areas. Thus, the threshold should be selected from the brightness ranging from 140 to 240. Incidentally, the average of the brightness for this image is given as 123.5. Fig. 5 (b) demonstrates the relation between the threshold and the mean whitecap coverage for 10 min in the time zone including the original image shown in Fig. 4. Here, the image processing has been made for the thresholds in 13 cases. The straight line drawn in the figure denotes the threshold of 175 adopted practically for this time zone. From this figure, it is observed that whitecap coverage begins to decrease gradually when the threshold exceeds 140; this critical value conforms well to that in Fig. 5 (a). In addition, the change in whitecap coverage for the threshold of 175 ± 10 becomes approximately $\pm 0.05\%$. The mean whitecap coverage in the threshold of 175 indicates 0.264%; the relative error against the change of ± 10 becomes about 18%. Therefore, it is concluded that the threshold-dependence of whitecap coverage for one image differ little from that of the mean coverage for 600 images, and that we can use a common threshold level through 600 images.

Images taken in the case where the sunlight was relatively high, so that it was difficult to distinguish the whitecapping area from the background, were removed from the objects of the analysis, that is, only what can provide whitecap coverage with sufficient accuracy was analyzed in this study. Thus, whitecap coverage in this study has a higher accuracy compared with existing data because of the use of averages over 600 images.

4. Results and discussion

4.1. Meteorological and wave-field conditions

The time series of the 10-m wind speed U_{10} , the wind direction WD, the significant wave height H_s , the peak wave period T_p , the peak wave direction D_p and the near-water air stability ΔT are displayed in Fig. 6 (a) and (b), which were acquired through the observations A and B, respectively. In these figures, the values of U_{10} and WD have been averaged over 10 min (2 points/h), and the air stability indicates the average over 10 min (6 points/h). In addition, the values averaged over 20 min are shown for H_s , T_p and D_p (1 point/h). First, let us investigate the wind and wave-field conditions for the

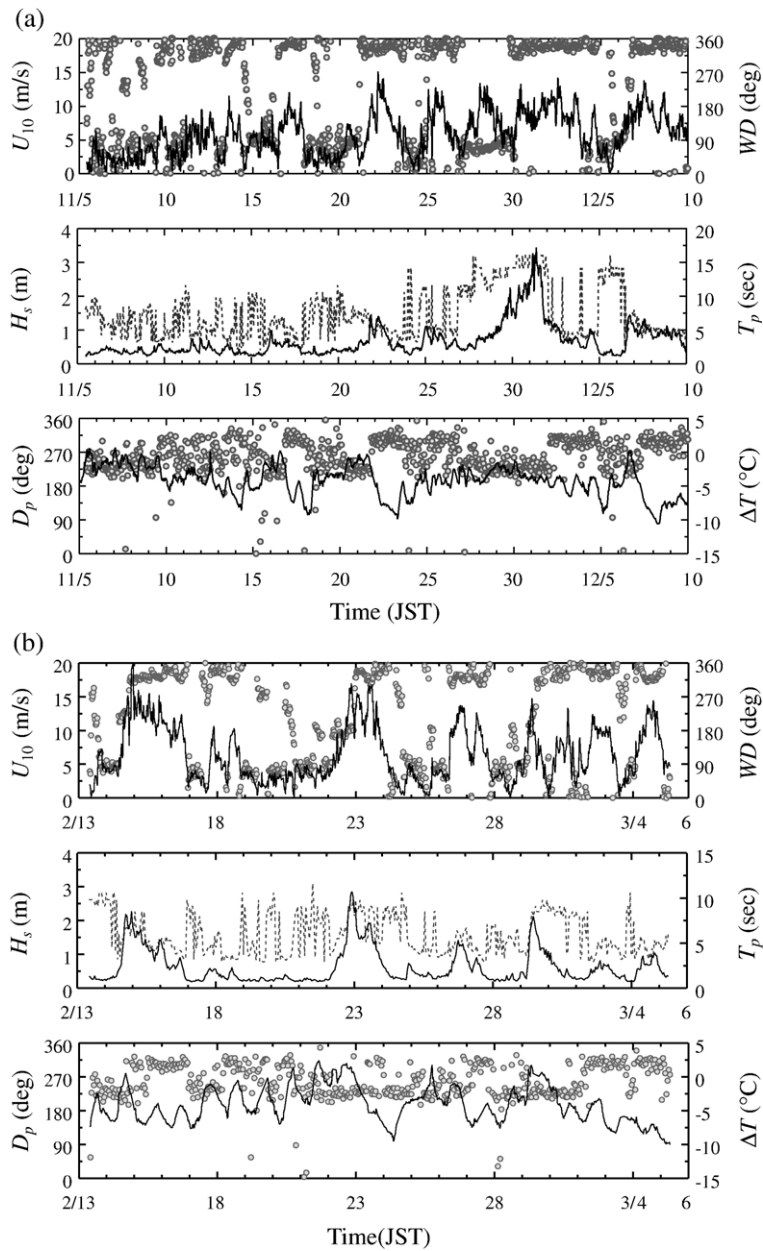


Fig. 6. Time series of meteorological and oceanographic data. (a) Observation A, (b) Observation B; 10-m wind speed U_{10} (solid line), wind direction WD (solid circles), significant wave height H_s (solid line), peak wave period T_p (dashed line), peak wave direction D_p (solid circles) and near-water air stability ΔT (solid line).

observation A. In the first half of the observation, U_{10} was relatively low, and H_s and T_p remained small, while they were increased in the latter half by a typhoon that approached from November 30 to the next day. These maximum values approximately were 15 m/s, 3 m and 16 s, respectively. There exist approximately two dominant wind directions, i.e., the north-northwesterly (NNW) and the easterly (E), which correspond to the

monsoon of winter and the land breeze, respectively. The propagating directions of the peak waves are found to be the southwesterly (SW) and the northwesterly (NW), where SW is the direction for swells propagating from the open sea, and NW indicates the propagating direction of wind waves generated by the monsoon. A long period swell propagating from SW apparently is recognized when the typhoon approached.

Table 1
Data summary

Date	Time (JST)	U_{10} (m/s)	U_{10N} (m/s)	u_* (m/s)	ΔT (°C)	H_s (m)	T_p (s)	c_{pw} (m/s)	W_C (%)	Class
<i>Observation A</i>										
2003.11.15	11:00	6.99	7.27	0.302	-4.86	0.27	2.0	3.12	0.0719	p
2003.11.20	09:00	6.86	7.01	0.286	-1.78	0.37	6.0	3.28	0.0412	c
2003.11.20	09:10	7.42	7.56	0.301	-1.67	0.37	6.0	3.28	0.0582	c
2003.11.20	11:00	6.56	6.65	0.212	-0.82	0.41	5.8	3.28	0.0277	x
2003.11.20	11:10	7.00	7.08	0.240	-0.81	0.41	5.8	3.28	0.0131	x
2003.11.20	12:10	7.17	7.26	0.235	-1.06	0.38	6.0	2.81	0.0201	c
2003.11.20	13:00	6.33	6.43	0.233	-0.97	0.45	6.4	3.59	0.0371	x
2003.11.20	13:10	7.36	7.44	0.214	-0.90	0.45	6.4	3.59	0.0373	x
2003.11.20	14:00	5.72	5.82	0.208	-0.92	0.48	6.7	3.74	0.0222	c
2003.11.20	14:10	5.81	5.90	0.206	-0.81	0.48	6.7	3.74	0.00430	c
2003.11.21	09:10	4.64	4.77	0.233	-1.24	0.54	6.0	4.37	0.00106	x
2003.11.23	09:00	8.36	8.74	0.383	-8.33	0.62	2.4	3.74	0.276	p
2003.11.23	09:10	8.58	8.95	0.381	-8.21	0.62	2.4	3.74	0.278	p
2003.11.23	10:00	7.58	7.96	0.403	-7.53	0.59	2.8	4.37	0.313	p
2003.11.23	10:10	7.28	7.66	0.384	-7.41	0.59	2.8	4.37	0.229	p
2003.11.30	09:10	11.79	11.99	0.504	-3.61	2.10	14	6.08	0.413	x
2003.11.30	10:00	9.95	10.16	0.376	-3.68	1.91	14	6.86	0.258	x
2003.11.30	10:10	9.46	9.69	0.474	-3.87	1.91	14	6.86	0.257	x
2003.11.30	11:00	9.42	9.63	0.350	-3.70	2.03	14	7.64	0.279	f
2003.11.30	11:10	8.79	9.02	0.389	-3.64	2.03	14	7.64	0.214	f
2003.11.30	12:00	10.02	10.23	0.453	-3.41	1.93	14	7.95	0.384	x
2003.11.30	12:10	10.26	10.46	0.419	-3.43	1.93	14	7.95	0.304	x
2003.11.30	13:00	10.26	10.47	0.443	-3.58	1.82	16	7.64	0.656	x
2003.11.30	13:10	9.86	10.07	0.468	-3.52	1.82	16	7.64	0.573	x
2003.11.30	14:00	9.66	9.87	0.392	-3.63	2.15	14	7.80	0.682	x
2003.11.30	14:10	8.75	8.98	0.435	-3.47	2.15	14	7.80	0.434	x
2003.11.30	15:00	9.63	9.82	0.408	-3.12	2.13	14	7.64	0.254	x
2003.11.30	15:10	9.48	9.67	0.402	-3.11	2.13	14	7.64	0.151	x
2003.12.01	09:00	9.26	9.49	0.370	-4.20	2.89	16	6.71	0.448	x
2003.12.01	09:10	8.89	9.13	0.373	-4.09	2.89	16	6.71	0.0762	x
2003.12.01	10:00	8.52	8.74	0.323	-4.02	2.92	16	7.49	0.363	x
2003.12.01	10:10	7.98	8.21	0.302	-4.09	2.92	16	7.49	0.126	x
2003.12.01	11:00	8.81	9.03	0.355	-3.81	2.60	16	7.49	0.320	x
2003.12.01	11:10	9.31	9.52	0.349	-3.53	2.60	16	7.49	0.421	x
2003.12.01	12:00	9.68	9.91	0.507	-3.73	2.81	16	7.64	0.264	x
2003.12.01	12:10	9.36	9.57	0.401	-3.63	2.81	16	7.64	0.348	x
2003.12.01	13:00	9.34	9.57	0.496	-3.66	2.90	16	6.39	0.632	x
2003.12.01	13:10	9.97	10.18	0.453	-3.54	2.90	16	6.39	0.518	x
2003.12.01	14:00	11.19	11.39	0.485	-3.61	2.87	16	5.61	0.931	x
2003.12.01	14:10	12.05	12.25	0.469	-3.78	2.87	16	5.61	0.649	x
2003.12.01	15:10	11.46	11.66	0.364	-3.90	2.26	16	5.46	0.452	x
2003.12.03	09:10	7.53	7.84	0.377	-5.42	0.59	4.4	6.86	0.299	p
2003.12.03	10:00	8.62	8.91	0.484	-4.79	0.63	4.5	7.02	0.480	p
2003.12.03	10:10	11.09	11.34	0.458	-4.80	0.63	4.5	7.02	0.862	p
2003.12.03	11:00	11.84	12.06	0.451	-4.49	0.72	3.9	6.08	0.919	x
2003.12.03	11:10	11.72	11.94	0.451	-4.46	0.72	3.9	6.08	1.13	x
2003.12.06	09:00	7.45	7.66	0.406	-2.75	0.36	12	3.28	0.0542	c
2003.12.06	10:00	5.88	6.10	0.295	-2.99	0.34	2.6	4.06	0.0738	p
2003.12.08	09:00	6.56	7.06	0.431	-10.40	0.80	5.3	8.27	0.236	p
2003.12.08	09:10	7.25	7.67	0.332	-10.34	0.80	5.3	8.27	0.291	p
<i>Observation B</i>										
2004.02.15	08:00	11.74	12.04	0.477	-6.89	1.28	6.2	8.42	0.780	x
2004.02.15	08:10	12.14	12.46	0.603	-6.87	1.28	6.2	8.42	0.928	x
2004.02.15	09:00	11.56	11.87	0.470	-7.09	1.29	8.5	5.15	0.723	x
2004.02.15	10:00	12.25	12.56	0.519	-6.83	1.46	5.1	6.24	1.08	f
2004.02.15	10:10	13.74	14.03	0.540	-6.88	1.46	5.1	6.24	0.970	f

Table 1 (continued)

Date	Time (JST)	U_{10} (m/s)	U_{10N} (m/s)	u_* (m/s)	ΔT (°C)	H_s (m)	T_p (s)	c_{pw} (m/s)	W_C (%)	Class
<i>Observation B</i>										
2004.02.16	09:00	8.53	8.89	0.454	-7.12	0.63	4.5	7.02	0.270	p
2004.02.16	09:10	11.35	11.69	0.555	-7.14	0.63	4.5	7.02	1.01	p
2004.02.23	08:10	11.32	11.51	0.439	-3.70	1.50	8.5	6.71	0.620	x
2004.02.23	09:00	12.69	12.88	0.449	-3.90	1.74	5.1	7.95	1.08	x
2004.02.23	09:10	12.01	12.22	0.517	-4.03	1.74	5.1	7.95	0.825	x
2004.02.23	10:00	15.91	16.13	0.618	-4.98	1.73	5.5	8.58	2.16	x
2004.02.23	10:10	16.35	16.57	0.666	-5.28	1.73	5.5	8.58	1.69	x
2004.02.26	09:00	9.78	9.89	0.365	-1.37	0.45	5.3	4.21	0.350	x
2004.02.26	09:10	9.07	9.18	0.324	-1.28	0.45	5.3	4.21	0.520	x
2004.02.27	08:00	12.64	12.92	0.453	-6.55	0.82	4.2	6.55	0.850	p
2004.02.27	08:10	12.14	12.42	0.399	-6.64	0.82	4.2	6.55	1.59	p
2004.02.29	09:00	10.13	10.02	0.398	0.50	1.97	8.5	9.36	0.0850	f
2004.02.29	09:10	9.54	9.43	0.326	0.40	1.97	8.5	9.36	0.0700	f
2004.02.29	10:00	9.26	9.07	0.323	0.79	2.13	8.0	6.24	0.140	f
2004.02.29	10:10	9.82	9.65	0.386	0.82	2.13	8.0	6.24	0.160	f
2004.02.29	11:00	8.62	8.41	0.313	0.86	1.98	8.5	5.30	0.0900	f
2004.02.29	11:10	7.72	7.49	0.294	0.85	1.98	8.5	5.30	0.110	f
2004.03.01	08:00	6.98	7.22	0.273	-3.93	0.50	8.5	4.21	0.0900	x
2004.03.01	08:10	8.96	9.18	0.308	-4.23	0.50	8.5	4.21	0.205	x
2004.03.01	09:00	8.67	8.93	0.367	-4.48	0.55	9.1	4.21	0.205	x
2004.03.01	09:10	8.43	8.69	0.355	-4.55	0.55	9.1	4.21	0.425	x
2004.03.01	10:00	8.30	8.57	0.311	-5.41	0.47	8.0	4.37	0.280	x
2004.03.01	10:10	7.75	8.04	0.312	-5.52	0.47	8.0	4.37	0.145	x
2004.03.01	11:00	8.10	8.40	0.329	-6.01	0.38	8.5	4.21	0.175	x
2004.03.01	11:10	7.35	7.65	0.292	-6.08	0.38	8.5	4.21	0.125	x
2004.03.02	09:00	6.76	7.08	0.371	-5.19	0.30	8.5	3.74	0.0500	x
2004.03.02	09:10	6.68	7.00	0.367	-5.05	0.30	8.5	3.74	0.0550	x
2004.03.02	10:00	7.92	8.19	0.342	-4.82	0.34	2.9	4.52	0.105	p
2004.03.02	10:10	7.33	7.63	0.393	-4.85	0.34	2.9	4.52	0.0750	p
2004.03.03	08:00	5.73	6.12	0.275	-8.22	0.44	4.9	7.64	0.125	p
2004.03.03	08:10	6.02	6.40	0.265	-8.29	0.44	4.9	7.64	0.125	p
2004.03.03	09:00	5.08	5.49	0.275	-8.00	0.40	4.7	7.33	0.0600	p
2004.03.03	09:10	4.37	4.79	0.264	-7.96	0.40	4.7	7.33	0.0700	p
2004.03.04	09:00	9.88	10.22	0.406	-7.83	0.96	5.5	8.58	0.620	p
2004.03.04	09:10	9.20	9.58	0.480	-7.82	0.96	5.5	8.58	0.785	p
2004.03.04	10:00	10.14	10.47	0.385	-7.72	0.72	5.3	8.27	1.08	p

Symbols U_{10} and U_{10N} are: 10-m and 10-m neutral wind speeds respectively, u_* : friction velocity, ΔT : near-water air stability, H_s : significant wave height, T_p : peak wave period, c_{pw} : phase speed of dominant wind waves and W_C : whitecap coverage. The “class” column classifies our data as *pure windsea* (p), *counter swell* (c), *following swell* (f) or *cross swell* (x).

The near-water air stability ranged from -11 to 0 °C, that is, it took the negative values. This means that the state of the atmosphere close to the sea surface was almost unstable. On the other hand, in the observation B, the wind from NNW blew periodically at a strong wind speed of about 12 m/s. The maximum values of H_s and T_p became approximately 3 m and 12 s, respectively. We can find two dominant wind directions to be analogous to the case of the observation A. The peak wave directions were SW and NW, so that the wave-field conditions are also considered to be analogous to those found in the observation A. Since the near-water air stability in the observation B varied in almost the same range as the other period, all the present data were taken only in the case of the unstable or the neutral conditions.

The values of U_{10} , ΔT , H_s and T_p for the time zone when whitecap coverage W_C was obtained are given in Table 1.

As stated above, around the observation tower, as typical states of the wave field, the following cases are possible: (1) wind waves only propagate from E or NNW, (2) a swell propagating from SW is dominant and (3) both cases are superimposed. We examine relative relations between wind waves and swell on the basis of the directional frequency wave spectra. According to the deflection angle between the propagating directions of wind waves and swell, which have been determined from the directional frequency wave spectra, we classify our data into the following four groups: *pure windsea*, *counter swell*, *following swell* and *cross swell*. The data

for which wind waves could not be distinguished from swell were removed from the candidate for the analysis. *Pure windsea* stands for the case where there exist wind waves only in the wave field. *Counter swell* means that the deflection angle ranges above $\pm 135^\circ$, and *following swell* shows the deflection angle to be within $\pm 45^\circ$. Also, *cross swell* indicates that the deflection angle ranges from $\pm 45^\circ$ to $\pm 135^\circ$. This classification is based on the studies of Donelan et al. (1997) and Drennan et al. (1999). Examples of the directional wave spectra obtained from the WAVEADCP data are displayed in

Fig. 7 (a) to (d), which give the cases of *pure windsea*, *counter swell*, *following swell* and *cross swell*, respectively. The arrows in these figures indicate the wind azimuth vector. Even in the case of *pure windsea*, the propagating direction deviates somewhat westerly from the wind direction, and surface waves at various frequencies are superimposed on the windsea. In addition, the swell is mainly propagated from SW facing the open sea, so that the wind direction in the case of *counter swell* almost became easterly. Wind waves in this direction have not frequently been observed because the waves

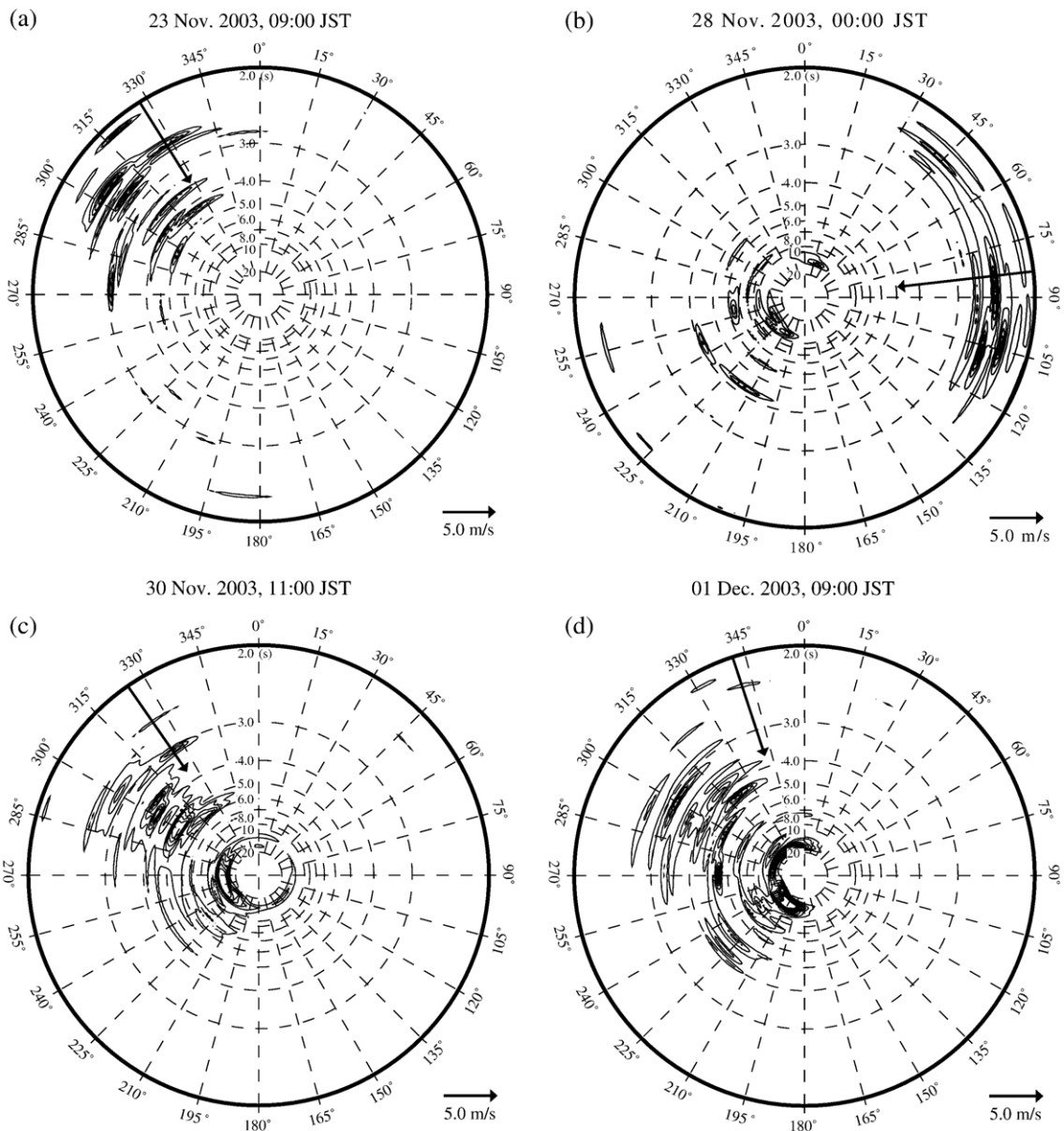


Fig. 7. Directional frequency wave spectra. (a) *Pure windsea*, (b) *counter swell*, (c) *following swell*, (d) *cross swell*.

might not be fully developed due to a short fetch. The classified relative relations between wind waves and swell are summarized in Table 1.

4.2. Wind-speed dependence

Fig. 8 shows whitecap coverage W_C plotted versus the 10-m wind speed U_{10} , where previous data and empirical expressions obtained by other researchers are also plotted (Monahan, 1971, 1993; Toba, 1972; Ross and Cardone, 1974; Snyder et al., 1983; Asher and Wanninkhof, 1998; Asher et al., 2002; Stramska and Petelski, 2003; Lafon et al., 2004). Our data, whose values are shown in Table 1, give an obvious behavior of whitecap coverage over a wide range of the wind speeds. For the wind speeds of $U_{10} > 7$ m/s, they are comparatively close to the empirical expression of Stramska and Petelski (2003). In a region of high wind speeds, W_C seems to be proportional to the cube of U_{10} , so that we can expect a linear relation between $W_C^{1/3}$ and U_{10} . The variation of $W_C^{1/3}$ with U_{10} is displayed in Fig. 9. $W_C^{1/3}$ increases linearly with increasing U_{10} over a wide range of the wind speeds though the data are somewhat scattered. Monahan (1993) proposed the relation between W_C and U_{10} as given by Eq. (1). From a linear regression of our data, the values of c_0 and $c_1^{1/3}$ become 2.01 and 0.093, respectively. The solid line in the figure indicates the regression with the correlation coefficient $r = 0.86$.

Phillips (1985) showed the dissipation rate of the wave energy to be proportional to the cube of the air friction velocity on the basis of the equilibrium spectrum of wind waves. The dissipation rate ε may be directly connected with wave breaking. If there exists a linear relation between W_C and ε , $W_C^{1/3}$ should be in proportion to u_* . The dependence of $W_C^{1/3}$ on u_* is shown in Fig. 10,

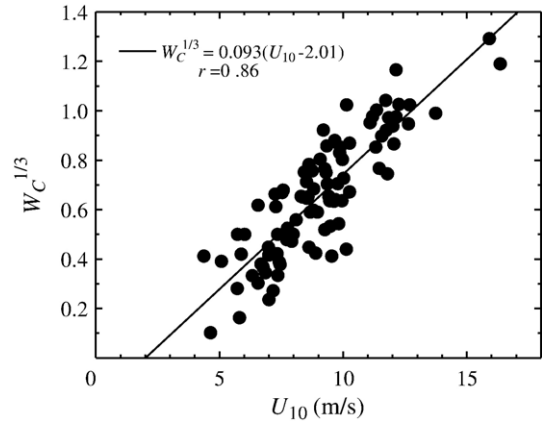


Fig. 9. Relation between $W_C^{1/3}$ and U_{10} .

which supports this hypothesis to be valid. However, although the correlation coefficient is comparatively high, the data scattering seems not to improve compared with Fig. 9. This is due to the error included in the evaluation of u_* itself. The friction velocity varies depending on the near-water air stability ΔT even in the same wind-speed conditions, so that U_{10} should be converted into the wind speed under the neutral condition U_{10N} . By using U_{10N} instead of U_{10} , we can expect to remove the influence of the air stability from the relation between whitecap coverage and wind speed. Therefore, in the following sections will be used the neutral wind speed U_{10N} . The values of u_* and U_{10N} are listed in Table 1.

4.3. Swell dependence

Fig. 11 shows the relation between $W_C^{1/3}$ and U_{10N} classified by the conditions of wind waves and swell, where the solid and dotted lines give linear regressions

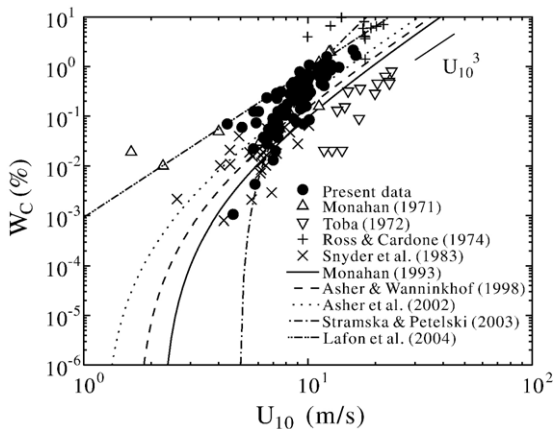


Fig. 8. Relation between W_C and U_{10} .

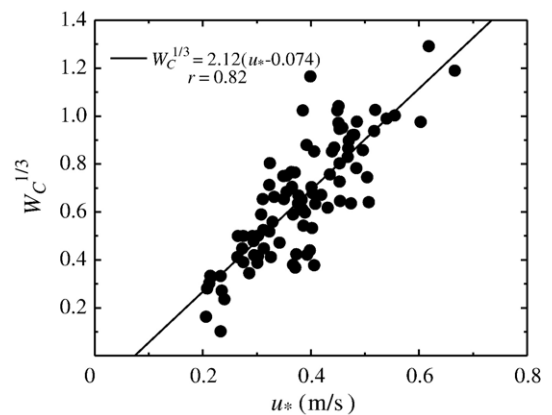


Fig. 10. Relation between $W_C^{1/3}$ and u_* .

for *pure windsea* and all the other data, respectively. We should note that the influence of the wave age has been still included in this relation, and that the data scattering has been caused by both the wave age and swell conditions. It is evident from the figure that whitecap coverage in the condition of *pure windsea* becomes large compared with the conditions including swell. This indicates that whitecaps are mainly ruled by wind waves and the whitecapping is suppressed by the presence of swell. Donelan et al. (1997) reported that the drag coefficient in the case of *counter swell* was larger than that for *pure windsea*. The increase of the coefficient, i.e., the momentum flux, may be thought to activate the generation of whitecaps. The observational results of Donelan et al. (1997) thus contradict the present ones such that these types of swells suppress the whitecapping. Since the wind in the case of *counter swell* must blow pushing back the swell, we may consider simply the drag coefficient to become large. However, the process of wave breaking shows the different behaviors. Though this difference may be closely connected with the interactions between wind waves and swell, the reason remains to be clarified. From this figure, it is difficult to find a certain relation between whitecap coverage and the deflection angle except for the deviation of *pure windsea* from the data including swell. This fact suggests that the influence of the deflection angle on wave breaking is very small, while whether there exists the swell on the windsea or not is important for the parameterization of whitecap coverage. We should note that the present data for relatively long swells correspond to “shallow water conditions”, though the condition of “deep water” is valid for wind waves. The wave steepness for long swells observed in this study approximately ranges from 0.002 to 0.02, which are based on the

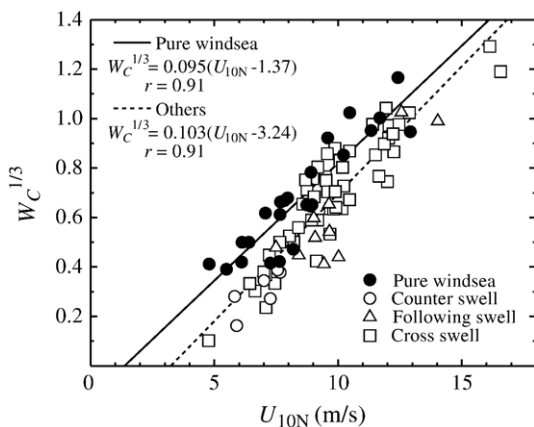


Fig. 11. Relation between $W_C^{1/3}$ and U_{10N} classified by the conditions of wind waves and swell.

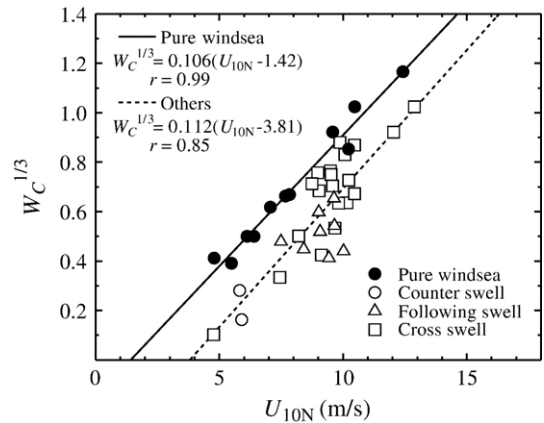


Fig. 12. Relation between $W_C^{1/3}$ and U_{10N} classified by the conditions of wind waves and swell in the case of $16 < c_{pw}/u_* < 29$.

significant wave height and the peak wavelength calculated from the small-amplitude wave theory. This means that the swell does not break due to the shoaling even in the shallow water condition. Since the presence of the sea bottom influences the swell propagation, the whitecapping may be affected indirectly by the sea bottom. However, it may be difficult to find the variation of the coverage depending on details of swell properties because it cannot be confirmed even in the relation with the deflection angle between wind waves and swell.

In order to quantify suitably the influence of swell condition, the relation of $W_C^{1/3}$ with U_{10N} should be discussed when the wave age c_{pw}/u_* remains fixed, where c_{pw} indicates the phase speed of dominant wind waves and the value is given in Table 1. For this reason, we classify the observational data into two groups based on the wave ages of $8 < c_{pw}/u_* < 16$ and $16 < c_{pw}/u_* < 29$. The threshold value of 16 has been chosen as an

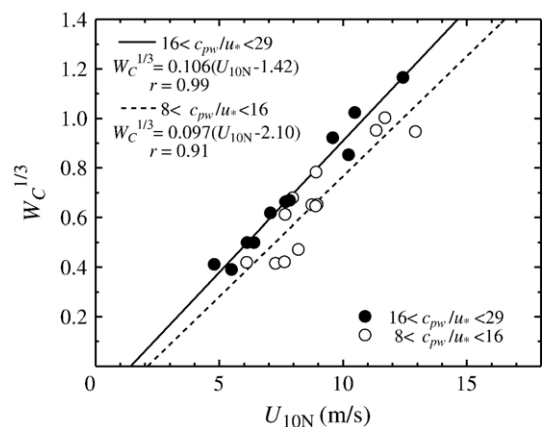


Fig. 13. Relation between $W_C^{1/3}$ and U_{10N} classified according to the wave age in the case of *pure windsea*.

intermediate one of the wave age within the range from 8 to 29. Also, the two groups have been so divided that the number of the data becomes approximately equal. In Fig. 12, the dependence of $W_C^{1/3}$ on U_{10N} is plotted only for the data of the wave age ranging from 16 to 29, where the solid and dotted lines are linear regressions by the least square method. These are the same types as the empirical expression given by Eq. (1); the values of c_0 and $c_1^{1/3}$ become 1.42 and 0.106 for *pure windsea*, and 3.81 and 0.112 for all the other cases, respectively. From this figure, the difference between the pure windsea and swell-affected windsea can be confirmed more clearly. The values of c_1 seem to be almost the same between both. Thus, we assume that the influence of swell appears only in the coefficient c_0 , which is the intercept along the U_{10N} -axis. It is concluded that the difference of whitecap coverage between the pure windsea and the cases including swell is equivalent to the wind speed of about 2.4 m/s. The influence should be treated to accurately parameterize whitecap coverage.

4.4. Wave-age dependence

Let us consider subsequently the influence of the wave age on whitecap coverage in the case where the swell condition remains fixed. Fig. 13 indicates the relation between $W_C^{1/3}$ and U_{10N} for *pure windsea* only. Thus, the influence of swell has been removed from this relation. The figure shows that in the same wind-speed condition, whitecap coverage is increased with increasing the wave age though the influence is relatively small compared with that by the presence of swell. This is due to the scale of breaking waves that becomes large as the wave age increases, and the dissipation rate of the wave energy is intensified. The values of $c_1^{1/3}$ in the regressions

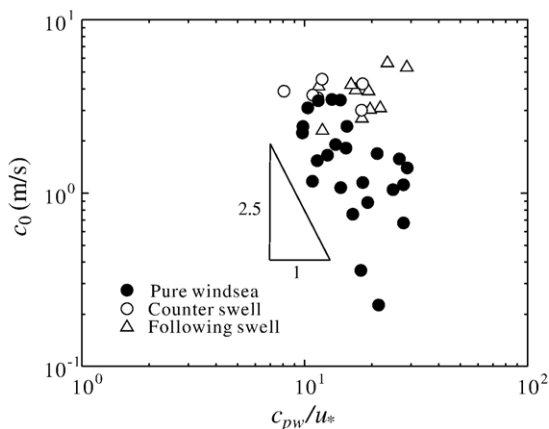


Fig. 14. Relation between c_0 and c_{pw}/u_* classified by the conditions of wind waves and swell.

take approximately about 0.1 regardless of the wave age. From the values of c_0 , the effect of the wave age converted into the wind speed is found to be 0.7 m/s.

As seen above, the influences of the wave age and swell condition can be quantified in terms of the coefficient c_0 , whereas we expect the value of c_1 to be approximately universal. Hence, the value of c_0 may become a function of the wave age and swell condition only. Fig. 14 shows the relation between c_0 and the wave age c_{pw}/u_* , which have been determined from the empirical expression assuming that $c_1^{1/3} = 0.1$. It is seen from the figure that in the case of *pure windsea*, c_0 decreases according to the -2.5 power of the wave age; this is consistent with the behavior that whitecap fraction increases with the fetch as pointed out by Woolf (2005). On the other hand, for the data including swell, the value of c_0 does not depend apparently on the wave age. This suggests that the presence of swell contaminates the fetch-dependence of whitecap coverage.

5. Conclusions

Whitecap coverage has been investigated on the basis of the wave-field conditions. The digital images of the sea surface were taken at the sea observation tower and whitecap coverage was computed accurately as the mean value over 600 images. Whitecap coverage W_C is proportional to the cube of the 10-m neutral wind speed U_{10N} in a range of high wind speeds and also proportional to the cube of the friction velocity u_* . The conditions of the wave field were distinguished according to the deflection angle between the propagating directions of wind waves and swell, which was identified by the directional frequency wave spectra. It is difficult to find a certain relation between whitecap coverage and the deflection angle. However, whitecap coverage under the condition of *pure windsea* is relatively larger than the coverage in the other conditions including swell. It is deduced from the behavior of W_C against the wave-field conditions that whitecaps are produced most actively in the case of *pure windsea* and the presence of swell suppresses the generation of whitecaps. It is concluded that whitecap coverage also increases with the wave age under the same wind-speed conditions.

Acknowledgements

The authors thank Profs. N. Matsunaga and A. Masuda for their helpful discussions. Thanks are extended to D. Furutera for his technical help. This work has been partially supported by Grant-in-Aid for Scientific Research from Japan Society for the Promotion of Science.

References

- Asher, W.E., Wanninkhof, R., 1998. The effect of bubble-mediated gas transfer on purposeful dual-gaseous tracer experiments. *J. Geophys. Res.* 103, 10555–10560.
- Asher, W.E., Higgins, B.J., Karle, L.M., Farley, P.J., Sherwood, C.R., Gardiner, W.W., Wanninkhof, R., Chen, H., Lantry, T., Steckley, M., Monahan, E.C., Wang, Q., Smith, P.M., 1995. Measurement of gas transfer, whitecap coverage and brightness temperature in a surf pool: an overview of WABEX-93. In: Jähne, B., Monahan, E.C. (Eds.), *Air–Water Gas Transfer*. AEON, pp. 205–216.
- Asher, W.E., Edson, J., McGillis, W., Wanninkhof, R., Ho, D.T., Litchendorf, T., 2002. Fractional area whitecap coverage and air–sea gas transfer velocities measured during GasEx-98. In: Donelan, M.A., Drennan, W.M., Saltzman, E.S., Wanninkhof, R. (Eds.), *Gas Transfer at Water Surfaces*. AGU, pp. 199–203.
- Donelan, M.A., Drennan, W.M., Katsaros, K.B., 1997. The air–sea momentum flux in conditions of wind sea and swell. *J. Phys. Oceanogr.* 27, 2087–2099.
- Drennan, W.M., Kahma, K.K., Donelan, M.A., 1999. On momentum flux and velocity spectra over waves. *Boundary - Layer Meteorol.* 92, 489–515.
- Lafon, C., Piazzola, J., Forget, P., Lecalve, O., Despiau, S., 2004. Analysis of the variations of the whitecap fraction as measured in a coastal zone. *Boundary - Layer Meteorol.* 111, 339–360.
- McGillis, W.R., Edson, J.B., Ware, J.D., Dacey, J.W.H., Hare, J.E., Fairall, C.W., Wanninkhof, R., 2001. Carbon dioxide flux techniques performed during GasEX-98. *Mar. Chem.* 75, 267–280.
- Monahan, E.C., 1971. Oceanic whitecaps. *J. Phys. Oceanogr.* 1, 139–144.
- Monahan, E.C., 1993. Occurrence and evolution of acoustically relevant sub-surface bubble plumes and their associated, remotely monitorable, surface whitecaps. In: Kerman, B.R. (Ed.), *Natural Physical Sources of Underwater Sound*. Kluwer Academic Publishers, pp. 503–517.
- Monahan, E.C., Spillane, M.C., 1984. The role of whitecaps in air–sea gas exchange. In: Brutsaert, W., Jirka, G.H. (Eds.), *Gas Transfer at Water Surfaces*. D. Reidel, pp. 495–504.
- Phillips, O.M., 1985. Spectral and statistical properties of the equilibrium range in wind-generated gravity waves. *J. Fluid Mech.* 156, 505–531.
- Ross, D.B., Cardone, V., 1974. Observations of oceanic whitecaps and their relation to remote measurements of surface wind speed. *J. Geophys. Res.* 79, 444–452.
- Snyder, R.L., Smith, L., Kennedy, R.M., 1983. On the formation of whitecaps by a threshold mechanism. Part III: field experiment and comparison with theory. *J. Phys. Oceanogr.* 13, 1505–1518.
- Stramska, M., Petelski, T., 2003. Observations of oceanic whitecaps in the north polar waters of the Atlantic. *J. Geophys. Res.* 108, 3086, doi:10.1029/2002JC001321.
- Toba, Y., 1972. Local balance in the air–sea boundary processes. I. On the growth process of wind waves. *J. Oceanogr. Soc. Japan* 28, 109–120.
- Toba, Y., Koga, M., 1986. A parameter describing overall conditions of wave breaking, whitecapping, sea-spray production and wind stress. In: Monahan, E.C., Mac Niocaill, G. (Eds.), *Oceanic Whitecaps*. D. Reidel, pp. 37–47.
- Wolf, D.K., 2005. Parametrization of gas transfer velocities and sea-state-dependent wave breaking. *Tellus* 57B, 87–94.
- Zhao, D., Toba, Y., 2001. Dependence of whitecap coverage on wind and wind–wave properties. *J. Oceanogr.* 57, 603–616.